# SURFACE MODIFIED AND FUNCTIONALIZED MAGNETIC GRAPHENE OXIDE FOR PURIFICATION OF WATER: REVIEW AND ANALYSIS

**Anupama sharma[1], Savita Agarwal[2], Poonam Parihar[3], Nupur jain[4], Sumit Kumar Gupta[5], Palvi Jindal[6]***

**Article History: Received:** 16.05.2023 **Revised:** 27.06.2023 **Accepted:** 31.07.2023

**Abstract**

Water is an essential element for day to day activities like agriculture, industries and domestic uses etc for human beings. Now-a-days, water pollution by heavy metal is one of the major environmental problems. Various methods like chemical precipitation, ion exchange, membrane filtration, coagulation-flocculation, flotation and adsorption have been adopted for the removal of heavy metal ions from the water. Among all these methods adsorption process has been widely used for the removal of heavy metals due to its low cost, environment friendly nature and easy availability. The commercial adsorbents, bio-adsorbents and nano-sorbents possess high removal capacity, thus used for the removal of heavy metals from waste water treatment. In recent years nanosorbents used in environmental remediation as it possess large surface area and high substance specificity. The present review aims to assemble the role of functionalized graphene oxide for heavy metal removal from waste water. The presence of various functional groups on graphene oxide provides abundant sites and increase surface area which improves the adsorption efficiency of pollutants. Thus an attempt is made to emphasis on low cost adsorbent and search for the parameters that affects the adsorption of heavy metals on various adsorbents.

**Keywords:** Graphene oxide, Functionalization, Magnetic Nanocomposite, Heavy metals

[1,4,5]St Wilfred PG College, Jaipur, India – 302020
[2]Chatrapati Shivaji Maharaj University, Panvel, Navi Mumbai, India – 410221
[3]Maheshwari PG College Pratapnagar, Jaipur, India - 302017
[6]Department of chemistry, Amity University, Jaipur, India - 303007

**DOI: 10.31838/ecb/2023.12.Si8.548**

## 1. INTRODUCTION

Water is an essential natural resource. Rapid industrialization and urbanization have caused contamination of water by the heavy metals [1]. Heavy metal contamination is one of the most important environmental issues. The industrial waste water often contains cadmium, zinc, copper, nickel, lead, mercury and chromium etc[2]. Heavy metal ions released from electroplating[3] and metal-finishing industries[4] have accumulated in organisms through food chain and cause serious impacts on environmental ecosystem and human health by the physicochemical properties[5]. Heavy metals are non-biodegradable [6], their bioaccumulation in living organisms resulted in various diseases and disorders in human beings [7]. The long term exposure of heavy metals may lead damage of nucleic acids, cause mutation, mimic hormones by disrupting the endocrine and reproductive system ultimately lead cancer [8,9]. There are various conventional methods used for the removal of these toxic pollutants from the environment. Adsorption method has proven one of the most widely preferable used techniques for the removal of heavy metals from wastewater [10,11]. The high cost of efficient adsorbents in adsorption process increases the cost of wastewater treatment [12]. It is important to find efficient and cost-effective adsorbents for the removal of heavy metals from wastewater [13]. Thus, new technologies which lower the cost and footprint of the processes that purifies water resources are always remain in desperate demand [14-16]. Recently much research is focused on grapheme for different water treatment processes and nanotechnology also has great potential for elimination of bacteria and other contaminants [17,18]. Graphene has recently attracted much interest in the materials field due to its unique 2D structure and outstanding properties [19]. The synthesis of graphene-based nanocomposites had become one of the most important research frontiers in the application of grapheme [20,21]. These oxide-based nanoadsorbents considered as one among the best adsorbents as it possesses high surface area, less impact on environment, easy availability and nongeneration of secondary pollutants [22,23]. The oxide-based eco-friendly and high-cost nanoadsorbents have been employed for the degradation of industrial effluents as well as for the removal of hazardous heavy metal pollutants present in wastewaters[24,25]. Graphene oxide, the functionalized graphene with oxygen-containing chemical groups has recently attracted many interests of researchers due to its superior properties such as large surface area, mechanical stability, tunable electrical,and optical properties[26,27]. Magnetic nanoparticles is an emerging field of study and has gained much attention among researchers due to their widespread applications in various fields like catalysis , environmental remediation, data storage, electronic communication, magnetic fluids and biomedicine etc[27-33]. Among different types of magnetic nanoparticles, iron oxide nanoparticles are the most popular and widely used in the field of environmental remediation and biomedicine due to their ease of surface modification, synthesis and low toxicity[34]. The currently attracting magnetic graphene oxide based nanocomposites have been widely used as an efficient adsorbent of dyes and heavy metal ions from aqueous solution due to its good dispersion in water, biocompatibility, easy and cost effective preparation methods[35]. Functionalized graphene is regarded as a very promising nanomaterial owing to its superior hydrophilicity, mechanical stability, bacteriostasis, and biocidal properties [36,37]. The functionalization of graphene oxide with molecules containing strong chelating

groups significantly enhances the removal efficiency of graphene oxide based materials [38,39]. Citric acid is frequently used to deal with various pollutants as it is an excellent chelating agent, environmental friendly and low cost compound [40,41]. Citric acid act as immobilized insoluble catalysts and can be easily separated and reused. It is used to remove and discourage the buildup of lime scale from boilers and evaporators. Modification with Citric acid is used for elimination of various dyes and heavy metal ions from industrial effluent [42,43]. Thus, in the present review attempts have been made to provide the brief view on graphene based nanocomposites as nanosorbents, surface modification of magnetic graphene oxide, its synthesis and its application in removal of heavy metal ions from waste water.

**Synthesis of graphene oxide by oxidation of graphite:** The preparation graphene oxide was firstly reported by Brodie in 1859 [44] by performing reaction between graphite and $KClO_3$ in fuming $HNO_3$. In 1898 Staudenmaier[45] modified this method by adding the chlorate and increasing the acidity of mixture by concentrated $H_2SO_4$ as oxidizing agent as shown in Figure1.

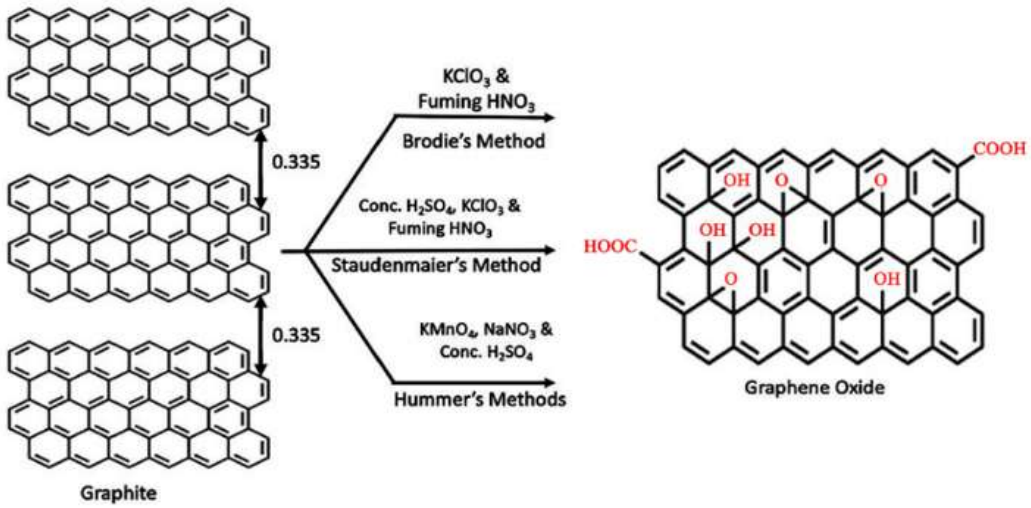


Figure 1: Schematic illustration of graphene oxide synthesis [46] by chemical oxidation using Brodie's, Staudenmaier's and Hummer's methods (For interpretation of the reference to color in this figure legend, the reader is referred to the Web version of this article).

The most popular Hummers-Offeman method [47] uses a water free mixture of concentrated $H_2SO_4$, $NaNO_3$, and $KMnO_4$. This method remains a key point of interest as it provides a good yield, carried out safely, requires less time than other previous methods and easier to produce large quantities of graphene oxide. Researchers have been focused to improve Hummers' method so that it becomes more efficient and environmental friendly as mentioned in Table1.

Table1: The summarized reported modified Hummers' methods.

| Carbon Source | Oxidant | Temperature (in °C) | Reaction Time Required | Features | Reference |
|---|---|---|---|---|---|

| | | | | | |
|---|---|---|---|---|---|
| Graphite powder | $H_2SO_4$, $K_2S_2O_8$, $P_2O_5$. | RT | 6 h. | Diode like behavior, highly conductive | 48 |
| Graphite flakes | $KMnO_4$, $H_2SO_4$, $H_3PO_4$ | 50 | 12h | Greater yield, not release toxic gases | 49 |
| Expanded graphite diameter ~15 μm | $KMnO_4$, $H_2SO_4$ | 90 | 1h 30 min | Safe, massive production | 50 |
| Graphite flakes | Conc.$H_2SO_4$/$H_3PO_4$, $KMnO_4$, $H_2O_2$ | 40-60 | 6-24 | green, safe , simple , and fully-oxidized GO preparation method | 51 |
| Graphite flakes | $H_2SO_4$, $KMnO_4$, $NaNO_3$ | 5-10 | 16 h | High quality, size confined upto 10 nm | 52 |
| Graphite flakes (3–20 um) | $H_2SO_4$, $KMnO_4$ | 20,40,95 | 1h | High yield, good quality, safe | 53 |
| Graphite flakes | $HNO_3$-$H_2SO_4$, $KMnO_4$ | 50 | 3h | Tri component acids, high yield | 54 |
| Graphite>10 um | $K_2FeSO_4$ | 100 | 1h | Ultra less cost, less pollution, recycling of $H_2SO_4$ | 55 |
| Defective arc-discharge carbon | $HNO_3$ | RT | 20 h | Nano sized GO | 56 |
| Graphite 44um | $KMnO_4$, $H_2SO_4$, $H_3BO_3$, $(NH_4)_2S_2O_8$ | ,5-35-95 | 5H | Less impurity, less acid, high yield | 57 |
| graphite | 98%$H_2SO_4$, fuming $H_2SO_4$ | RT | 3-4 h | Lightly oxidized, 25 nm thick, 100% conversion | 58 |
| Graphite foil | $H_2SO_4$ | RT | ,5min | Electrochemical support, high efficiency and | 59 |

| | | | | | |
|---|---|---|---|---|---|
| | | | | high yield | |
| graphite | $H_2SO_4$ $KMnO_4$, $H_3PO_4$ | <RT-35-95 | >24h | Cool the exo-thermal reaction, completely safe, no risk of explosion | 60 |
| MWCNTs ( 5 μm) | $HNO_3$,$H_2SO_4$,$K_2MnO_4$, $NaNO_3$, | RT | 2 h 30 min | Excellent durability, effective adsorption | 61 |
| Graphene oxide | PVDF, | 80 | 24h | Self healing property, good antifouling performance, high rejection ratio | 62 |
| Dried GO powder | EDC | RT, 150 | 1h | Suitable for microporous membranes | 63 |
| 2D nanochannels | $H_2SO_4$,$HNO_3$, laponite | RT | 24 h | High permeability, high rejection rate | 64 |

**Preparation of Magnetic graphene oxide**: Magnetite nanoparticle and graphene oxide were promising nanoparticles that can be used in variety of field due to their exceptional characteristic [65]. Graphene oxide has a unique 2-D structure and excellent chemical and physical characteristics [66] while magnetite nanoparticle has its superparamagnetic properties[67] which enable it to be controlled by external magnetic field. The extensive survey of literature reveals three general methods for the synthesis of magnetic nanoparticle functionalities with graphene oxide [68] were hydrothermal method, direct pyrolysis and co-precipitation. Several reported methods have been discussed following for the synthesis of magnetic graphene oxide.

***Pyrolysis*:** The MP/GO nanocomposites were synthesized [69] by mixing GO water suspension with $Fe(NO)_3$ in different precursor amounts at 70 °C with 300 rpm magnetic stirring. GO: $Fe(NO)_3$ =10:1, 5:1, 1:1, and 1:5, products labeled as MP/GO10, MP/GO5, MP/GO1 and MP/GO0.2, respectively. The synthesized MP/GO nanocomposites as shown in Figure 2 were filtered and washed with distilled water. After that the annealing process was performed by heating GO up to 800 °C for 2 hrs under $H_2$ atmosphere balanced with 95% argon.

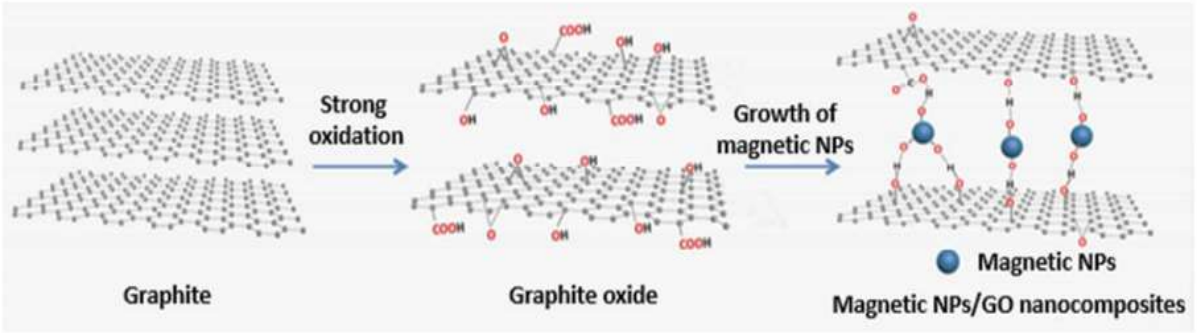


Figure 2: The diagrammatic presentation for synthesis of magnetic Nano particles (For interpretation of the reference to color in this figure legend, the reader is referred to the Web version of this article).

***Co-Precipitation:*** In this technique [70] graphene oxide is dispersed in deionized water, using ultrasonic irradiation for 5 min in the presence of nitrogen atmosphere. Then, mixture of $FeCl_3$.6H2O and $FeSO_4$.7H2O in distilled water was added to the graphene oxide solution and irradiated ultrasonically for 30 min. Addition of 25% $NH_4OH$ aqueous solution in the above mixture GO-$Fe_3O_4$ nanocomposite was readily separated.

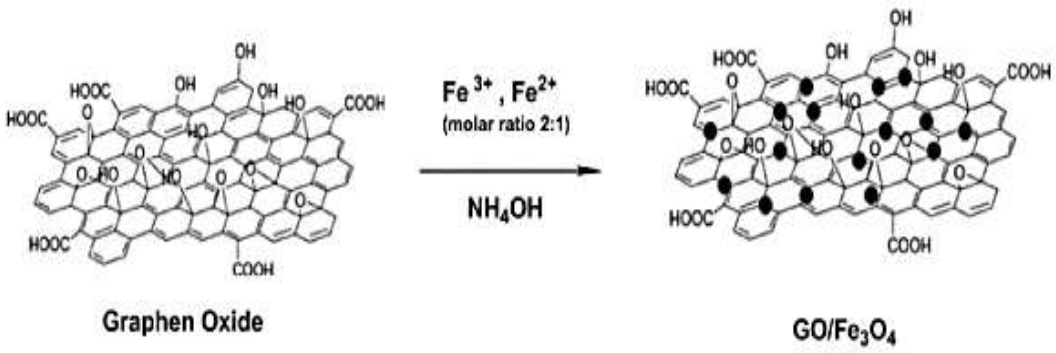


Figure 3: A schematic diagram for the synthesis of modifying $Fe_3O_4$-graphene oxide nanocomposite[71] (For interpretation of the reference to color in this figure legend, the reader is referred to the Web version of this article).

Magnetite nanoparticles were synthesized [72] by mixing of iron (II) and iron (III) salts in the molar ratio of 1.1 to 2 and filtered into fresh water using a microfilter of 0.2 µm pore size. Then addition of NaOH solution was in 10% excess to the doubly diluted iron salt solution in two portions, the first half slowly and the second half rapidly under rigorous stirring. After washing with water acidified the mixture with HCl solution and hydrothermal ageing of stable suspension in an ultrasonic bath at 80°C for 30 minutes was done. The mixing of suspensions of the magnetic iron oxide and the graphite oxide were used for the formation of composite materials. These suspensions were sonicated for 30 s before rapidly mixing them in appropriate volumes.

***Emulsion Method*:** Magnetic graphene oxide was synthesized by the reported [74] simple emulsion method in which graphene oxide was mixed with different amount of iron oxides. Firstly graphene oxide was mixed with chloroform and oleylamine for about 1 h through sonication process. Then, iron oxides were sonicated in chloroform solution for about half an hour. After that these two solutions were mixed together by using probe sonicator for 30 min in an ice bath for forming a homogenous solution. The final product was obtained after drying homogenous solution in an open air for 2 h and it was stored inside the dessicator.

***Hydrothermal Treatment*:** Functionalized magnetic graphene oxide nanoribbons composite material was synthesized [75] by hydrothermal treatment method using graphene oxide nanoribbons as raw material, which was added into ethylene glycol and sonicated for 6 h. $FeCl_3 \cdot 6H_2O$ and sodium acetate were added to the above mixture and stirred for 30 min. The mixture was transferred to a Tefon lined stainless steel reactor at 200 °C for 6 h which was placed in a controlled box furnace. Then, this mixture cooled to room temperature. The reaction product was washed repeatedly with deionized water and ethanol, and dried under vacuum at 60 °C for 12 h.

***In situ synthesis***: In situ synthesis [76] of the hybrid nanomaterial GO-γFe by dispersion of graphene oxide and [Fe(Nitrate)] in ethanol separately. Then these two solutions were mixed with stirring for 30 min. After that the mixture was heated at 100°C under continuous stirring for 1 h. Now cool this mixture at room temperature, so that hybrid nanoparticles were centrifuged and washed with ethanol several times, to clean the nanoparticles from any impurities.

***Solvothermal Method*:** In this system [77] ferric trichloride hexahydrate ($FeCl_3.6H_2O$) was added into ethylene glycol under magnetic stirring for complete dissolution. The aqueous suspension of graphene oxide was dispersed into the above solution with continuous magnetic stirring. The ammonium hydroxide was added to the solution by continuous dipping method. Polyvinylpyrrolidone was added slowly as the uniform mixture of the solution formed. The above mixture was pour into six teflon reactors for 20 h at 180 °C. After that, the reactors were cooled naturally and then the prepared mGO was separated by magnetic separation method and washing by mixture of ultrapure water and ethanol.

Another procedure followed to synthesized magnetic graphene oxide by solvothermal method [78] which involved mixture of $FeCl_3 \cdot 6H_2O$, PEG and anhydrous sodium acetate in ethylene glycol and allowed to stirring for 30. Graphene oxide was added into this solution after that transferred into a stainless steel autoclave at 180 °C temperature for 8 h. Finally prepared magnetic graphene oxide based material was washed with ethanol for three times and dried in vacuum at 40 °C.

**Synthesis of citric acid functionalized magnetic graphene oxide:** The presence of oxygen functionalities at graphene oxide surface is very important since they provide reactive sites for chemical modification using known carbon surface chemistry [79]. In this frame functionalized magnetic graphene oxide emerging as a versatile material for applications in nanoscience and nanotechnology [66].

The preparation of GO-g-PCA via a radical polymerization followed by a reported [80] procedure (Figure 4), in which three different amounts of graphene oxide were mixed with monohydrate citric acid to obtain a gray colored powder and transferred it into a double neck round bottom flask. The obtained mixture was heated up to 120 °C for 30 min under vigorous stirring, then the temperature was raised to 150 °C, at which the product was

melted. After 60 min, the temperature was raised to 160 °C and further stirred for 90 min to finish the reaction. Finally, the obtained product was dissolved in small amount of THF and precipitated in minimum amount of cyclohexane.

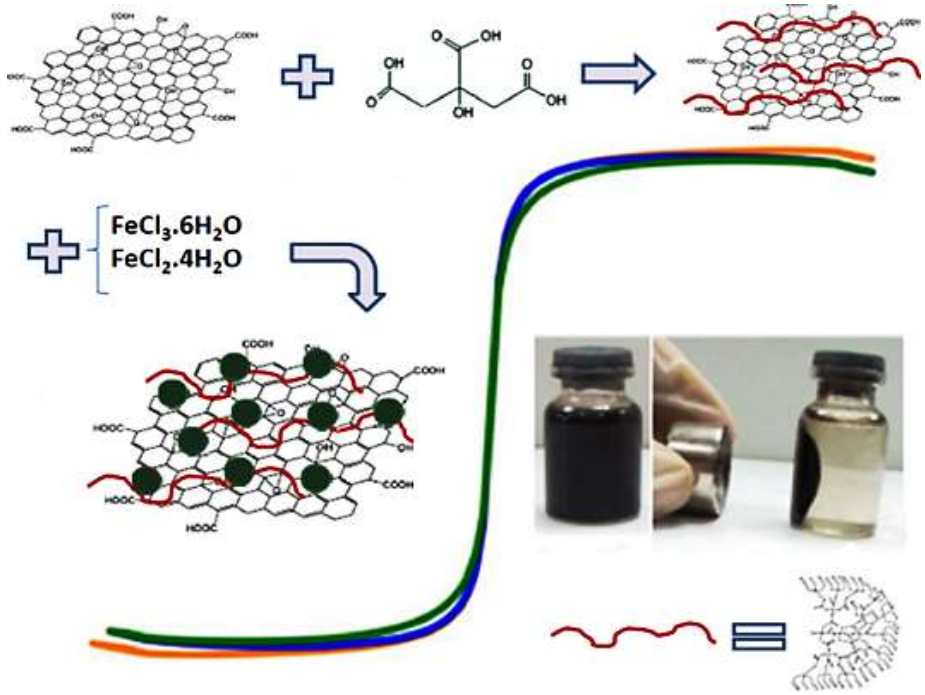


Figure 4: The diagramatic synthesis of highly magnetic nanocomposites consists of magnetite nanoparticles, graphene oxide and hyper-branched poly citric acid (For interpretation of the reference to color in this figure legend, the reader is referred to the Web version of this article).

Heyi Ge et al have been reported [81] the synthesis of citric acid functionalized magnetic graphene oxide coated corn straw (CA-mGOCS) as a new adsorbent. The magnetic graphene oxide was synthesized by solvothermal method. Then, citric acid has been added in magnetic graphene oxide coated corn straw to synthesize citric acid functionalized magnetic graphene oxide coated corn straw (CA-mGOCS). The magnetic graphene oxide in addition with 5 g and 10 g corn straw (CS) fiber was used to synthesize mGO5CS and mGO10CS.

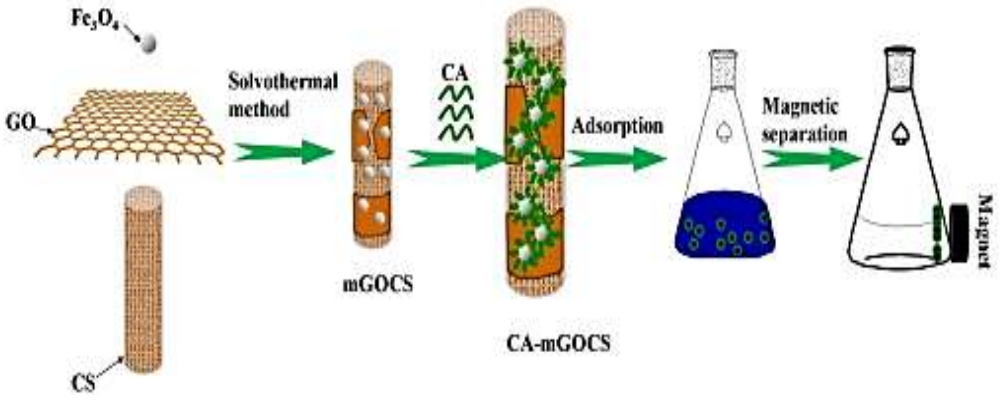


Figure 5: The schematic illustration of preparing CA-mGOCS and adsorption Methylene Blue process (For interpretation of the reference to color in this figure legend, the reader is referred to the Web version of this article).

Citric acid functionalized graphene oxide was synthesized [82] through an esterification reaction between GO-COCl and citric acid. To prepare acyl chloride-functionalized GO (GO-COCl), graphene oxide was dispersed in dry N,N'-dimethylformamide for 1 hour and then treated with $SOCl_2$ at $80^0$C for 3 days. After that under argon atmosphere citric acid in THF and $Et_3N$ were added to GO-COCl at 0°C temperature with continuous stirring for 1 hour. At room temperature 6h refluxing give GO- citric acid hybrid which was magnetized by co-precipitation method as shown in Figure 6.

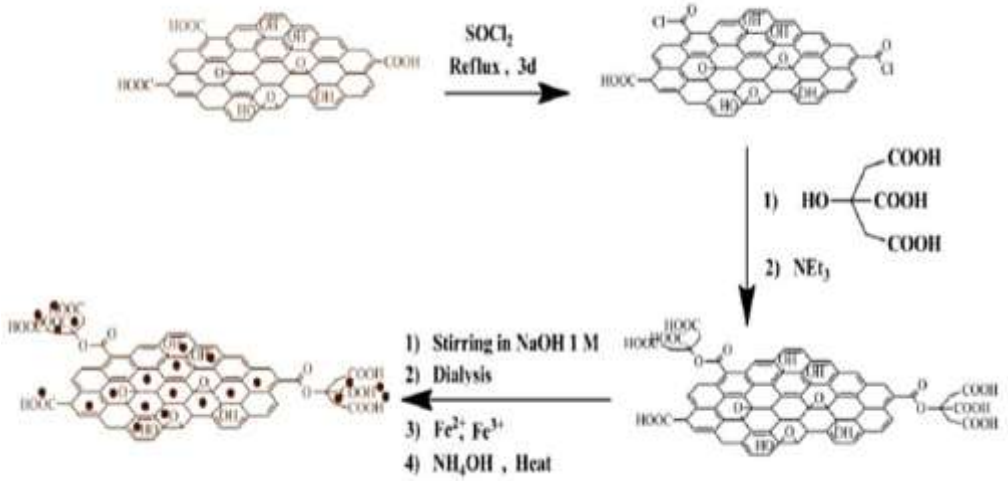


Figure 6: The procedure for preparation of magnetic citric acid grafted graphene oxide (For interpretation of the reference to color in this figure legend, the reader is referred to the Web version of this article).

The reported method[83] for modification of surface of graphene oxide by citric acid as shown in figure 7. This surface modified graphene oxide by citric acid used as a heterogeneous nanocatalyst in organic condensation reaction between alkyl substituted benzaldehyde and o-phenylenediamine to synthesize imidazole

derivatives in high yields and short reaction time at room temperature. The catalyst exhibits high catalytic activity and can be reusable. The efficient immobilizing of citrate groups on the surface of graphene oxide sheets was shown by the easy purification of catalyst for at least six cycles without significant loss of activity.

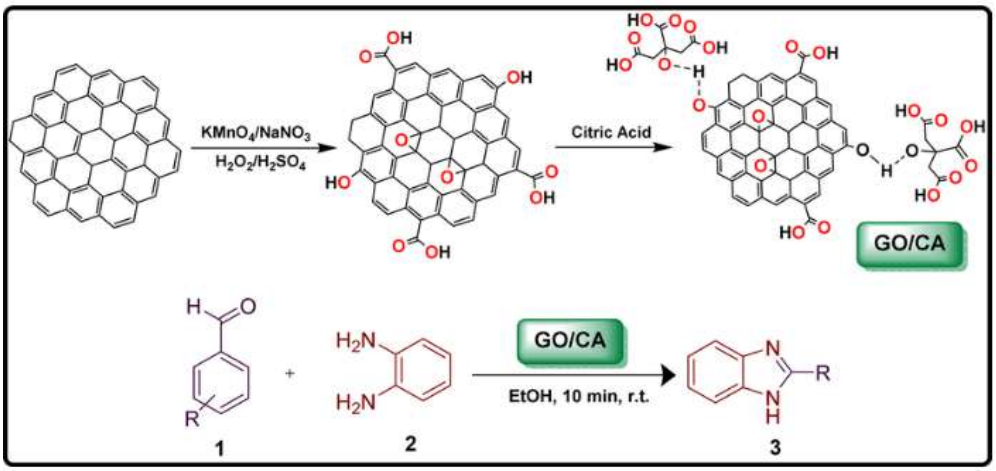


Figure 7: The schematic diagram for surface modification of graphene oxide by citric acid and its application as a heterogeneous nanocatalyst in organic condensation reaction (For interpretation of the reference to color in this figure legend, the reader is referred to the Web version of this article).

**Characterization**: The morphology and structure of citric acid functionalized magnetic graphene oxide were characterized by transmission electron microscopy (TEM) and scanning electron microscopy (SEM) as shown in Figure8. The average size determined from SEM images is 25 nm[82]. TEM morphology and size distribution of GO-CA-$Fe_3O_4$ nanocomposite were observed from micrographs (Figure8 (b)). The magnetic particles were well shaped spherical and not much agglomeration seen which implies that GO-CA can efficiently stabilize the magnetic nanoparticles. The TEM image indicates the mean size of the magnetic nanoparticles was found to be 25 nm which is consistent with the average particle size calculated from the Scherrer's relation in the XRD pattern [82].

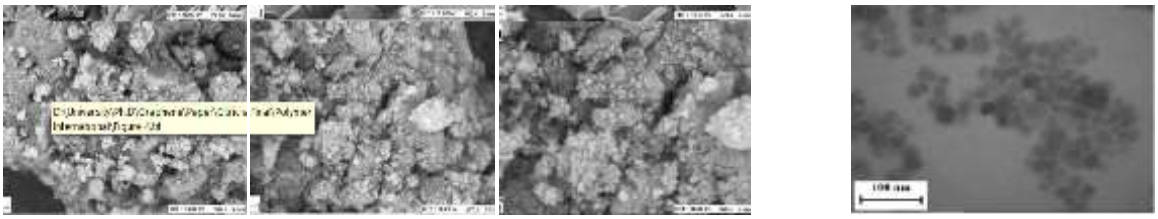

(a) (b)

Figure 8: SEM images for (a) GO-CA-$Fe_3O_4$ and (b) TEM images for GO-CA-$Fe_3O_4$ (For interpretation of the reference to color in this figure legend, the reader is referred to the Web version of this article).

The structures were measured by Fourier-transform infrared spectra analyzer and X-ray diffraction (XRD). XRD analysis was used to determine the average crystalline properties of the graphene oxide. The graphene oxide sheet in XRD

analysis showed a very strong peak at $2\theta$ = $10.2^0$ as shown in Figure 9 (a) which indicates the successful synthesis of GO sheet. The characteristic peaks assigned at 2θ values of 18.34° (1 1 1), 29.93° (2 2 0), 35.49° (3 1 1), 43.12° (4 0 0), 56.99° (4 2 2), and 62.52° (5 1 1) for GO-CA-$Fe_3O_4$ nanocomposite[82].

The FTIR spectra analysis was used to investigate the structure and presence of functional groups in citric acid functionalized magnetic graphene oxide. The graphene oxide sheet exhibited adsorption bands for the carboxyl C=O (1723 $cm^{-1}$), aromatic C=C (1621 $cm^{-1}$), epoxy C–O (1220 $cm^{-1}$), alkoxy C–O (1043 $cm^{-1}$), and hydroxy –OH (3391 $cm^{-1}$) groups (in Figure9 (b)) [82]. The presence of oxygen-containing functional groups like C=O and C–O further confirmed that the graphite indeed was oxidized into graphene oxide which was consistent with the literatures. The appearance of C=C groups showed that even graphite had been oxidized into graphene oxide the main structure of layer graphite was still retained.

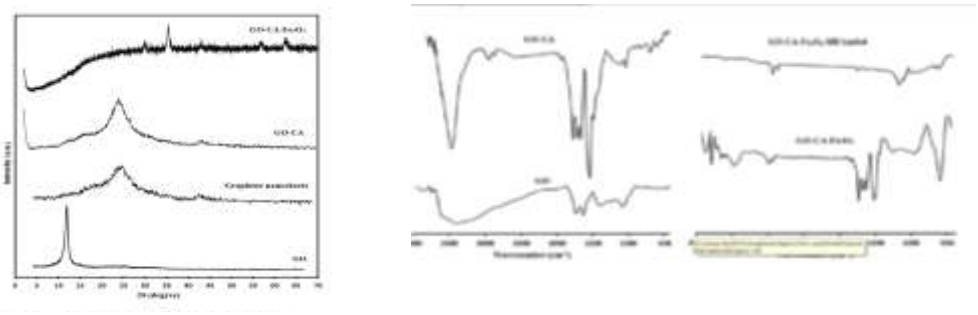

(a) (b)

Figure 9: The (a) XRD and (b) FTIR spectra of graphene oxide(GO), GO-CA, GO-CA-$Fe_3O_4$ and GO-CA-$Fe_3O_4$/MB- loaded (For interpretation of the reference to color in this figure legend, the reader is referred to the Web version of this article).

The peak at 3391 $cm^{-1}$ in graphene oxide spectrum assigned for hydroxy –OH group was reduced in broadness and shifted to 3431 $cm^{-1}$ due to esterifaction of hydroxy groups of graphene oxide and the carboxylic groups of citric acid. The absorbtion band at 1740 $cm^{-1}$ may be assigned for the ester and the new bands present at 2927 $cm^{-1}$ were asigned to $CH_2$ groups of citric acid. The signals of C=O in carboxylic acids of citric acid were appeared at 1694 and 1647 $cm^{-1}$. The charactristic peak of $Fe_3O_4$ was observed at 580 $cm^{-1}$ in the FTIR spectrum of GO-CA-$Fe_3O_4$. The bands attributed to carboxylic acid groups of citric acid were reduced in intensity and shifted to lower wavenumbers indicates the binding of a citric acid radical to the surface of $Fe_3O_4$ nanoparticles by chemisorptions of citrate ions [84]. The peak appeared at 3500 $cm^{-1}$ was significantly reduced in intensity as –OH groups of graphene oxide and –COOH groups of citric acid interact with magnetic nanoparticles.

The UV-VIS analysis [85] of the graphene oxide sheet and Magnetic graphene oxide was used to measure the optical absorption properties as shown in Figure 10(a) which indicated that graphene oxide possessed a good photoresponse not only in ultraviolet range but also in visible range (380-800 nm) which implied the enormous potential for application of light. The UV absorption peak of graphene oxide appeared at 238 nm assigned for the $\pi \rightarrow \pi^*$ transition of aromatic C-C bonds. In UV-vis absorption spectra of graphene oxide there was a broad band observed at 300 nm corresponding to the $n \rightarrow \pi^*$

transition for carbonyl bonds. The characteristic peak of Magnetic graphene oxide present at 300 nm as shown in Figure 10(b). This red shift of the peak from 238 nm to 300 nm is due to the introduction of $Fe_3O_4$ particles on the surface of graphene oxide.

The results of thermogravimetric analysis (TGA) and derivative thermogravimetric (DTG) analysis of the synthesized GO-g-PCA nanocomposites [80] are mentioned in Figure 10. The thermal properties of the nanoproducts and their compositions can be investigated by TGA analysis. The temperature range from 30 to 600˚C $Fe_3O_4$ shows about 2.1% mass loss and the decrease of mass can be attributed to the evaporation of surface water of magnetic particles. The weight loss below 180 ˚C may be assigned to the evaporation of solvent adsorbed on the surface due to hydrophilicity of graphene oxide [86]. In the temperature range 180-220˚C there is a rapid weight loss of the sample due to decomposition of the polymeric chains as well as detachment of the surface functional groups such as hydroxyl and carboxyl from the surface. In the temperature range 150-600 ˚C, the weight loss of GO-g-PCA was about 68.7%, 74.0% and 74.6% respectively for a, b and c curves in Figure 10(b), which was more in comparision of the graphene oxide sample (~34.2%) reported in the literatures [87] confirming that PCA is surely grafted on GO layers. [88]. The results showed that by increasing the amount of graphene oxide in the GO-g-PCA nanocomposite increases thermal stability.

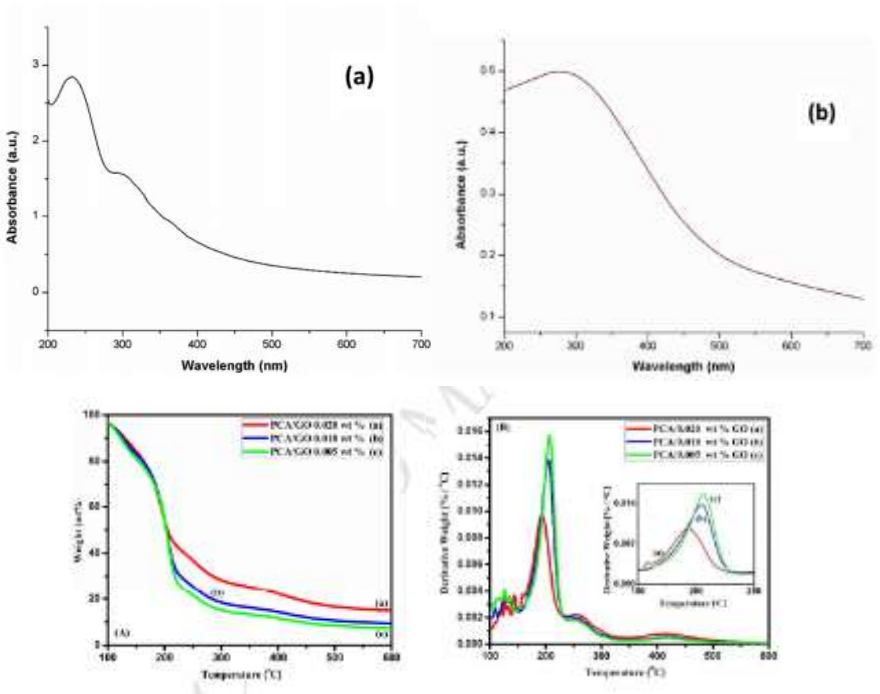


(c) (d)

Figure 10: (a) The UV-VIS spectra of graphene oxide sheet (b) The UV-VIS spectra of Magnetic graphene oxide (c) TGA analysis of synthesized GO-g-PCA with three different amounts of GO (d)DTG analysis (For interpretation of the reference to color in this figure legend, the reader is referred to the Web version of this article).

The Raman spectrum of synthesized GO-g-PCA nanocomposite[80] gives complementary information on the quality of synthesized graphene oxide. The characteristic G band of $sp^2$ carbon atom vibrations of graphite is

observed at 1581 $cm^{-1}$, in the case of graphite oxide, the G-band becomes broader and is shifted to 1594 $cm^{-1}$. The reduction of $sp^2$ domains and level of oxidation on the surface is indicated by D-band at 1363 $cm^{-1}$ [86,89]. In Figure 11, the D-band of the synthesized GO-g-PCA nanocomposite is at 1342 $cm^{-1}$ and the G-band is at 1602 $cm^{-1}$. The ID/IG ratio, larger than 1.098, indicates increased amount of structural defects. Here, this ratio is about 0.83, thus confirming the good quality of synthesized graphene oxide.

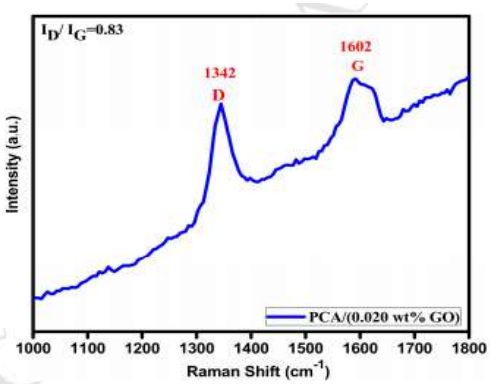


Figure 11: Raman spectrum of GOi-g-PCA nanocomposite (For interpretation of the reference to color in this figure legend, the reader is referred to the Web version of this article).

Nuclear magnetic resonance (NMR) spectroscopy $^1$H-NMR & $^{13}$C-NMR spectra provide structural imformation of GO-g-PCA nanocomposite [80]. The $^1$H-NMR spectra of GO-g-PCA (Figure 12(a)) contain two signals at 4.68 and 3.49 ppm may be assigned for the protons of –COOH and –OH groups, respectively. The signals in the range of 2.59-2.80 ppm and 3.22-3.48 ppm are related to protons of citric acid units in the polymer. The $^{13}$C-NMR spectra of GO-g-PCA (Figure 12(b)) the signals at 168.19-176.44 ppm indicate the presence of different carbonyl groups. The C=C carbons of graphene oxide were present at 129.13 and 139.11 ppm in the form of weaker signals. The signals of citric acid were observed at 73.07, 67.67 and 43.07 ppm [90].

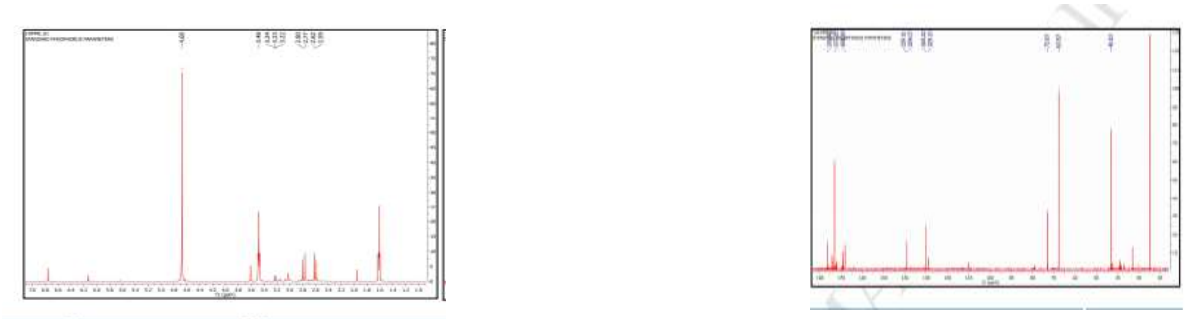

(a) (b)

Figure 12: (a) $^1$H-NMR and (b) $^{13}$C-NMR analysis of synthesized GO-g-PCA (For interpretation of the reference to color in this figure legend, the reader is referred to the Web version of this article).

XPS analysis was conducted to demonstrate the presence of oxygen-containing functional groups. XPS spectrum of the Magnetic graphene oxide

composite[85] showed significant C 1s, O 1s, and Fe 2p siognals corresponding to the binding energy of about 285, 530, and 711 eV. In the spectrum of Fe 2p (the inset of Figure 13), the peaks of Fe 2p3/2 and Fe 2p1/2 are shift at 711.27 and 724.74 eV from 710.34 and 724.02 eV in comparision of $Fe_2O_3$ peaks. The significant peak of C signal with a binding energy of 285.0 eV, which can be attributed to the C=C, C–C and C–H functional groups. The peak centered at the binding energies of 532.1 eV can be assigned to the C–O and C=O bonds. This result suggested that graphene oxide sheet contains large numbers of functional groups on its surface such as C–O and C=O, which also was in accordance with the XRD, FTIR, analyses.

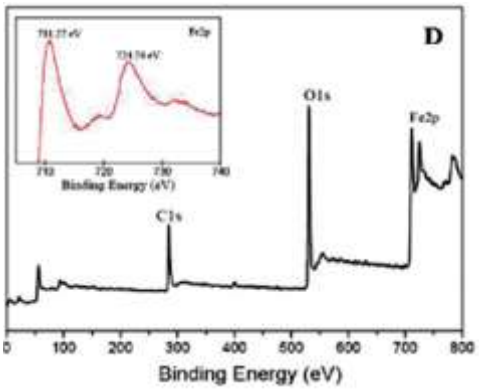


Figure 13: XPS spectrum of the M/GO composite (the inset illustrates the high-solution spectrum of the Fe 2p peak of the composite) (For interpretation of the reference to color in this figure legend, the reader is referred to the Web version of this article).

M-H curve was measured for the GO-Fe (50:50) where magnetization (M) as a function of applied field (H) with milling times of 25, 35, 40 and 45 h at room temperatures as shown in Figure 14. M-H curves exhibited superparamagnetic nature for GO-Fe. The saturation magnetization for the 25 h milled sample was the highest with a value of 78 emu/g. The decrease in iron amount in the resulting composition leads decrease of saturation in magnetization of the nanocomposites with an increase in milling time from 25–40 h. The decrease in the magnetization from milling times of 40 and 45 h was due to the size effect which can be attributed to the magnetically disordered surface spins, higher milling times makes the magnetic nanoparticles finer.

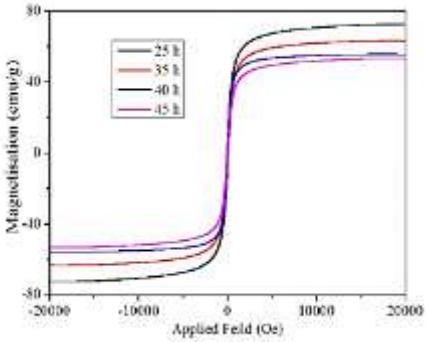


Figure 14: Magnetic hysteresis curves obtained for GO-Fe nanocomposite with a 50:50 composition milled for 25, 35, 40, and 45 h [91] (For interpretation of the reference to color in this figure legend, the reader is referred to the Web version of this article).

**Applications of Magnetite Nanoparticles for Heavy Metal Removal from Wastewater:** The functionalization of graphene oxide enhances its excellent properties as well as its adsorption capacity for the removal of heavy metal ions from the wastewater [92]. The carboxylates have important impact on the growth of magnetic nano particles and their magnetic properties, citric acid is one of the most suitable and easily available materials used to stabilize nano particles by coordination of one or two of the carboxylate functionalities. Citric acid grafted graphene oxide has been easily dispersed in water as it reduces the hydrophobic nature of nano particles to stablize them and adsorb the pollutants to form stable complexes.

The GO-CA-$Fe_3O_4$ nanocomposite [82] has great potential in removing organic dyes and can be easily separated by removal of dyes in the presence of an external magnetic field. The GO-CA-$Fe_3O_4$ nanocomposite was employed as an adsorbent of methylene blue from contaminated water and take 30 min to attain equilibrium. The adsorption capacity of nanocomposite in the concentration range studied was 112 mg $g^{-1}$as shown by adsorption isotherm in Figure 15 (a). The parameters like contact time, solution pH and temperature affect the adsorption isotherm of Methylene blue. The electrostatic interaction plays an important role in comparision of π-π stacking in adsorption of Methylene blue by nanocomposite. GO-CA has additional carboxylic groups that make the electrostatic interaction between MB and GO-CA more intense as mentioned in Figure15

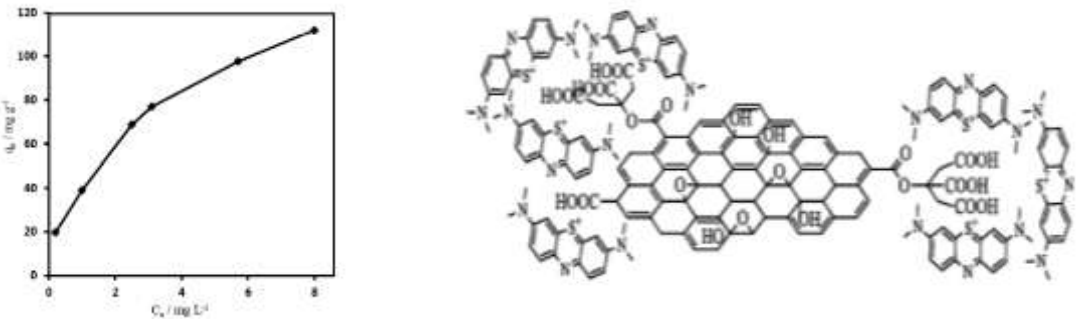


(a) (b)

Figure15: (a) Adsorption isotherm of methylene blue on GO-CA-$Fe_3O_4$ (temperature25˚C, contact time:30 min) (b) The schematic showing possible interaction of GO-CA/MB (For

interpretation of the reference to color in this figure legend, the reader is referred to the Web version of this article).

The novel, cost-effective and high-efficiency citric acid modified magnetic graphene oxide coated corn straw (CA-mGOCS) has been reported by Ge et. al [81]as an adsorbent for removal of methylene blue. Here, mGOCS (magnetic graphene oxide corn straw) was synthesized using a simple one-step solvothermal method and then citric acid was decorated on mGOCS by adjusting the reaction pH, temperature and reaction time. CA-mGO5CS had the better adsorption performance than other adsorbents. The maximum adsorption capacities in initial Methylene Blue concentration of 1000 mg $L^{-1}$ are 276.5 mg $g^{-1}$, 300.3 mg $g^{-1}$ and 315.5 mg $g^{-1}$ according to CA-mGO, CA-mGO10CS and CA-mGO5CS, which indicated that CA-mGO5CS has the best adsorption performance than others. The pseudo-second-order model and the Freundlich described the well adsorption behavior. The equilibrium adsorption capacity was 315.5 mg $g^{-1}$ for Methylene Blue at pH=12 and 298 k. The electrostatic incorporation as well as hydrophobic interactions between CA-mGO5CS and Methylene Blue determined the favourable adsorption property.

Furthermore, facile and cost-effective method has been reported [93] which possess the electrostatically driven co-assembly for the fabrication of a novel functional hybrid composed of graphene oxide wrapped $Fe_3O_4$ nanoclusters. The $Fe_3O_4$@GO nanohybrids reported in this study are synthesized by making use of the weak electrostatic interaction between negatively charged graphene oxide nanosheets and positively charged $Fe_3O_4$ nanoclusters. The thin and flexible graphene oxide shells effectively infold the $Fe_3O_4$ nanocluster core and formed $Fe_3O_4$@GO hybrid. The adsorptive removal efficiency of $Fe_3O_4$ @GO hybrid composite was investigated by using two model cationic dyes methylene blue (MB) and rhodamine B (RhB) and one model anionic dye methyl orange (MO) in relation to pH, adsorbent dosage, contact time, initial dye concentration and temperature. The adsorption kinetics and the equilibrium adsorptions were well-fitted with pseudo-second order kinetic model and Langmuir isotherm model, respectively. The maximum adsorption capacities of $Fe_3O_4$@GO nanohybrids for MB, RhB and MO were found to be 131.10, 34.50 and 39.95 mg/g respectively at 303 K temperature. The $Fe_3O_4$@GO adsorbent exhibited rapid magnetic separation, excellent stability, easy regeneration and good sustainability in removal efficiency even after continued recycling. It is found that the removal of both cationic and anionic dye pollutants in environmental remediation $Fe_3O_4$@GO composite possesses great potential as an efficient and recyclable adsorbent.

The magnetic functionalization of graphene oxide possesses unique properties like magnetic separation, chemical stability and forming stable complexes with pollutants. Some researchers have developed magnetic graphene oxide composites for efficient applications, including water treatment, energy storage and drug delivery. The use of magnetic materials for water purification can overcome the difficulties in filtration and regeneration of adsorbents. A novel magnetic nanocomposite $Fe_3O_4$/GO [94] has been successfully synthesized through one-step chemical coprecipitation method. The nanocomposite possess many intriguing properties such as chemical stability, high adsorption capacity, and superparamagnetic. These properties evoked great interest of its exploration in magnetic solid-phase extraction of heavy

metal ions from complex samples. The sample pH, amounts of adsorbent, sample volumes, elution volumes, and coexisting ions are several parameters which affect the analytical performance of nanocomposite. The adsorbed metal ions were easy eluted by controlling the pH condition and the materials could be reused more than 20 times. The limits of detection under the optimized conditions were found to be 0.016, 0.046, 0.395, 0.038, 0.157 μg $L^1$ for Co2þ, Ni2þ, Cu2þ, Cd2þ, and Pb2þ, respectively. The intra-day relative standard deviations were in the range of 1.8–5.5% at 10 μg $L^1$. The proposed method was successfully applied to biological sample (urine and plasma) analysis and got excellent recoveries in the range of 81–113% even the matrix was complex. The material displayed high adsorption capacity for five heavy metal ions and was stable even in acid solution. The adsorbent ability increased in high pH, which showed higher adsorption capacity for Cu2þ and Pb2þ due to the strong complexation ability with carboxylic groups. It could be separated rapidly under external magnet, reused at least 20 times, and successfully applied to MSPE. The method was fast, precise, easy to operate, and had low LODs.

The potential adsorption applications toward heavy metal ions and organic dyes were evaluated for GO–$Fe_3O_4$ hybrids [95] due to remarkable magnetic properties, great dispersibility and large specific surface area. $Cu^{2+}$ is one of common heavy metal ion contaminants in wastewater and lead toxicity, slow biological degradation and biological accumulation. Methylene blue is another most common colored chemical agent and regarded as one of the considerable pollutants cause massive environmental problems and very poisonous to human body. The effect of contact time for removal of $Cu^{2+}$ (adsorbate) using GO–$Fe_3O_4$ hybrid as adsorbent was evaluated as shown in Figure16(a) whereas the effect of contact time for removal of Methylene blue by GO– $Fe_3O_4$ was displayed in Figure16(b). The adsorption capacity of GO–$Fe_3O_4$ hybrids gradually increased with the increase of contact time. The maximum adsorption capacity of GO–$Fe_3O_4$ hybrids for $Cu^{2+}$ was found to be 18.1 mg/g and for Methylene blue it is about 23.2 mg/g.

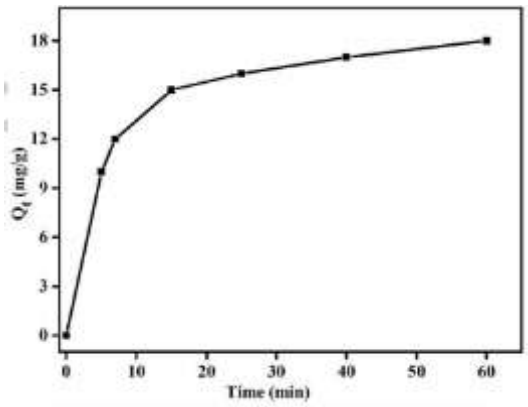


Figure 16: Time profile of $Cu^{2+}$ adsorption onto GO–$Fe_3O_4$ hybrids (initial $Cu^{2+}$ concentration 10 mg/L; solution pH 7; dose 10 mg and room temperature) (For interpretation of the reference to color in this figure legend, the reader is referred to the Web version of this article).

The synthesized Magnetic graphene oxide composites [96] were used as a versatile adsorbent for As (V) removal from aqueous solutions. The adsorption of As(V) on Magnetic graphene oxide is an endothermic process and the adsorption

kinetic well fitted for the pseudo-second-order model. The Magnetic graphene oxide composites shows good adsorption capability for As(V) removal and the adsorption isotherms were described by the Langmuir model better than by the Freundlich model. The adsorption of As(V) on Magnetic graphene oxide decreased with ascending pH due to the electrostatic interaction. The nature and concentration of coexisting cations and anions greatly affected the adsorption of As(V) on Magnetic graphene oxide. The Magnetic graphene oxide-bound As(V) can be quickly separated and recovered from aqueous solution by an easy magnetic separation method.

The one-pot synthesis of magnetic porous hydrogel[97] showed the efficient removal of arsenic and the superior regeneration. The maximum sorption capacities were estimated as 25.1 mg $g^{-1}$ for As (III) and 74.2 mg $g^{-1}$ for As (V) under neutral circumstance, respectively. Magnetic porous hydrogel maintained the satisfied sorption properties for As (III) and As (V) if the concentrations of competitive anions were 100 times as higher as arsenic concentrations. The presence of cations promotes the immobilization of As (V) and inhibited the sorption of As (III) on magnetic porous hydrogel. The excellent stability of magnetic porous hydrogel guaranteed its multiple recycling. Magnetic porous hydrogel was a potential candidate for the application in arsenic decontamination and incorporating assembly and chemical bubble was demonstrated to be a reliable strategy to facilely fabricate 3D porous hydrogel.

**Conclusions and future perspectives**: The review strongly defends citric acid functionalized magnetic graphene oxide and magnetic graphene oxide can be treat as advance adsorbent materials for the hazardous heavy metals and dyes present in waste water. Graphene oxide based materials have shown rapid and high hazardous pollutant organic molecules and heavy metals removal capability. The presence of remarkable mechanical, electrical, thermal, and barrier properties, graphene-based nanocomposites become a hot area of research. It has strong affinity, due surface complexation, electrostatic attraction, and ion exchange mechanisms which collectively improves its removal capacity and make it suitable for waste water treatment. Moreover, modifications in graphene oxide with citric acid has improve its adsorption capacity, selectivity, thermal and chemical stability and also facilitate the magneto-responsive separation of exhausted adsorbents from water. There is plenty of oxygen atoms present on surface of graphene oxide which gives a negative charge and Methylene Blue is a basic cationic dye and heterocyclic aromatic chemical compound thus it is likely to interact with negatively charged compounds like graphene oxide. The citric acid functionalized magnetic graphene oxide has additional carboxylic groups that make the electrostatic interaction with Methylene Blue more intense. In future, more innovative research works have to be explored in reference to convenient separation and regeneration of the magnetic graphene oxide based adsorbents. Graphene-based nanobiocatalyts are suitable for use in various applications, such as immobilization of enzymes in the field of biotechnology and biomedicine.

## 2. REFERENCES

1. H. Ali, E. Khan, and I. Ilahi, Hindawi J. Chem., 2019, **2019**, 1-14
2. M. A. Baraka, Arabian J. Chem. , 2011, **4** , 361-367
3. D. Sharma; P. K. Chaudhari; S. Dubey; and A. K. Prajapati, Environ. Eng. J., 2020, **146(10)** , 1-16.
4. A. Baral [a] and R. D. Engelken[b], Environ. Sci. & Policy, 2002, **5(2)**, 121-133.

5. A. Singh and S. M. Prasad, Int. J. Environ. Sci. technol., 2015, **12(1)**, 353-566.
6. Azimi, Azari, M. Rezakazemi, and M. Ansarpour, Chem. Bio. Eng., 2017, **4(1)**, 37-59.
7. M. Jaishankar, T. Tseten, N. Anbalagan, B. B. Mathew, and K. N. Beeregowda, Interdisciplinary Toxicology, 2014, **7(2)**, 60-70.
8. D. C. Malik, C. k. Jain and A. K. Yadav, Applied water sci. , 2017, 7, 2113-2136.
9. W. C. Leung, M. F. Wong, H. Chua, W. Lo and C. K. Leung , Water Sci. technol., 2000, **41(12)**, 233-240.
10. T. A. Kurniawan, G. Y. S. Chan, W. H. Lo and S. Babel , Sci. Total Environ , 2005, **366(2-3)**, 409-426.
11. D. Lakherwa, Int. J. Environ. Res. Dev., 2014, **4(1)**, 41-48.
12. K. C. Khulbe and T. Matsuura, Applied Water Sci., 2018, **8(1)**, 1-30.
13. R. k. Gutam, A. Mudhoo, G. Lofrano and M.C.Chattopadhyaya, J. Enviro. Chemical Eng., 2014, **2**, 239-259.
14. S. D. Gisi, G. Lofrano, M. Grassi and M. Natarnicola, Sustainable mater. & Technologies, 2016, **9**, 10-40.
15. H. Sadegh, G. A. M. Ali, V. K. Gupta, A. S. H Makhlouf, R. S. ghoshekandi, M. N. Nadagouda, M. Sillanpää and E. Megiel , J. nanostructure in chem., 2017, **7**, 1-14.
16. M. Naushad , A New Generation Material Graphene : Applications in Water Technology, Springer, **2019.**
17. P. Rajapaksha, A. Power, S. Chandra and J. Chapman, The Analyst, 2018, **143(23)**, 5629-5645.
18. P.G.Tratnyek and R.L.Johnson, Nano today, 2006, **1(2)**, 44-48.
19. Y. Lao and X. Li, Adsorption, 2014, **20**, 713-727.
20. P. Jayakaran, G. S. Nirmala, and L. Govindarajan, Hindawi Int. J. Chemical Eng., 2019, **2019**, 1-17.
21. Z. Terzopoulou, G. Z. Kyzas, and D. N. Bikiaris, Materials(Basel), 2015, **8(2)**, 652-683.
22. E. Weidner and F. Ciesielczyk, Mater., 2019, **12(6)**, 927.
23. V. B. Cashin, D. S. Eldridge, A. Yu and D. Zhao , Environ Science : Water research & Technology , 2018, **4(2)**, 110-128.
24. K. Da, H.U. Wen-Bin, Mater., 2013, **28(3)**, 235-246.
25. V. K Gupta, I. Tyagi, R. S. ghoshekandi and H. Sadegh, Sci. Technology & Development , 2015 , **34(3)** ,195-214.
26. F. Lia , X. Jianga , J. Zhaoa and S. Zhang, Nano Energy , 2015, **16**, 488-515.
27. U. K. Sur, Int. J. Electrochem. , 2012, **2012**, 1-12.
28. Rossi, L.M. Costa, N.J.S. Silva and F.P. Wojcieszak, R. Green Chem , 2014, **16**, 2906-2933.
29. Zhang, H. W. Liu and Y. Sun, Front Phys. Chin. , 2010 , **5(4)** , 347-356.
30. Tang and S. C. N. Lo, Water Res. , 2013 , **47** , 2613-2632.
31. S. Laurent , Dutz, S. Hafeli and U.O. Mahmoudi, Adv. Colloid Interface , 2011, **166**, 8-23.
32. .Li, X.-B. Gao, Y.-J. Wang, Y.Zhan, F. Zhang, X.-Y. Kong, Q.-Y. Zhao, N.-J. Guo, Q. Wu and H.-L. Li, J. Am. Chem. Soc. , 2017, **139**, 4789-4796.
33. Reddy, L.H. Arias, J.L. Nicolas and J. Couvreur, Chem. Rev. , 2012 , **112** ,5818-5878.
34. A. C. Lokhande, I. A. Qattan, C. D. Lokhande and S. P. Patole, J. Mater. Chem., 2020, **3**, 918-977.
35. N. H. Abdullah,K. Shameli, E. C.Abdullah and L. C. Abdullah**,** Composites B : Eng. , 2019 , **162**, 538-568.
36. X. Wang, Y. Zhao, E. Tian, J. Li, and Y. Ren, Advanced Mater. Enterface , 2018 , **5(15)** , 1701427-1701447.

37. F. S. Awad, K. M. AbouZied, W. M. Abou El-Maaty, A.M.E Wakil and M.S. El-Shall, Arabian J. chem. , 2020 , **123(10)** , 2659-2670.
38. K. Asemave, Organic and Medicinal Chem. Int. J. , 20178 , **6(4)** , 1-10.
39. N. J.Dixon, Handbook of Green Chemistry: Desining Safer Chemicals , Wiley , 2012 , **9** , 218-307.
40. D. Kolodynska, Environ. Sci. & Pollution Research Int. , 20132 , **20(9)** , 5939-5949.
41. B. Karimi, F. Mansouri and H. M. Mirzaei, Soc. Euro. J. Catalysts , 2015, **7(12)**, 1736-1789.
42. H. A. Hegazi, HBRC J. , 2013 , **9(3)**, 276-282.
43. M. Namvari and H. Namazi, Polymer Int., 2014 , **63(10)**, 1881-1888.
44. Brodie, Philos. Trans. R. Soc. Lond., 1859 , **149**, 249-259.
45. Staudenmaier, Ber. Dtsch. Chem. Ges., 1898 , **31**, 1481-1487 .
46. A. Adetayo, and D. Runsewe, J. Composite Mater., 2019 , **9** , 207-229.
47. Hummers and W. S. Offeman, J. Am. Chem. Soc., 1958 , **80(6)** , 1339.
48. Kovtyukhova, N. I. Ollivier, P.J. Martin, B.R. Mallouk, T.E. Chizhik, S.A. Buzaneva and E.V.Gorchinskiy, Chem Mater. , 1999 , **11** , 771-778.
49. D. C. Marcano, D. V. Kosynkin, J. M. Berlin, A. Sinitskii , Z. Sun and A. Slesarev , ACS nano , 2010 , **4(8)** , 4806-4814.
50. L. Sun and B. Fugetsu , Mater. Letters , 2013 , **109** , 207-210.
51. S. Peng, X. Fan, S. Li and J. Zhang , J. Chil. Chem. ,2013 , **58(4)** , 2213-2217.
52. S. Eigler , M. E. Heim , S. Grimm , P. Hofmann ,W. Kroener and A.Geworski , Adv. Mater., 2013 , **25(26)** , 3583-3587.
53. J. Chen , Y. Li , L. Huang , C. Li and G. Shi , Carbon , 2015 , **81** , 826-834.
54. V. Panwar , A. Chattree and K. Pal , Systems & Nanostructures , 2015 , **73** , 235-241.
55. L. Peng , Z. Xu , Z. Liu ,Y. Wei , H. Sun and Z. Li, Nature Communications , 2015, **6**, 5716.
56. L. M. Rosillo and C. G. Salzmann, Carbon, 2016, **106** , 56-63.
57. H. Yu , B. Zhang , C. Bulin , R. Li and R. Xing , Scientific reports, 2016 , **6** , 36143.
58. A. M. Dimiev ,G. Ceriotti , A. Metzger and N. D. Kim , ACS Nano, 2016, **10(1),** 274-279.
59. S. Pei , Q. Wei , K. Huang , H.-M. Cheng and W. Ren , Nature Communications, 2018, **9(1)**, 145.
60. P. Ranjan , S. Agrawal , A. Sinha ,T. R. Rao , J. Balakrishnan and A. D. Thakur , Scientific Reports, 2018, **8(1)**, 12007.
61. M. Musielak, A. Gagor, B. Zawisza, E. Talik and R. Sitko, ACS Applied Mater. & Amp. Interfaces, 2019,**11(31)**, 28582-28590.
62. R. Chang, S. Ma, X. Guo, J. Xu, C. Zhong, R. Huang and J. Ma, ACS Applied Mater. & Amp. Interfaces, 2019 , **11(49)**, 46251-46260.
63. T. Lee and B.-S. Kim., ACS Applied Mater. & Amp. Interfaces, 2020, **12(11)**, 13116-13126.
64. J.-Q. Hu, Z. Liu, Z.-H. Chen, Q.-W. Cai, X.-Y. Li, R. Xie, X.-J. Ju, W. Wang and L.-Y. Chu, Industrial & Amp; Eng. Chem. Research, 2020, **59(27)**, 12441-12450.
65. E. L. Albert, M. B. Sajiman and C. A. C. Abdullah , Applied Nanoscience, 2019, **9**, 43-48.
66. S. Priyadarsini, S. Mohanty, S. Mukherjee, S. Basu and M. Mishra, J. Nanostructure in Chem., 2018, **8**, 123-137.

67. J. Wallyn, N. Anton, and T. F. Vandamme, Pharmaceutics , 2019, **11(11),** 601.
68. L. Nánai, D. Nesztor, B. Barna, O. Malina,[2] and E. Tombácz, Advances in Mater. Sci. & Eng., 2018, **2018**, 11.
69. Y. Wang, Q. He, H. Qu, X. Zhang, J. Guo, J. Zhu, G. Zhao, H. A. Colorado, J.f. Yu, L. Sun, S. Bhana, M. A. Khan, X. Huang, D. P. Young, H. Wang, X. Wang, S. Wei, and Z. Guo, J. Mater. Chem. C , 2014, **58(4)**, 2213-2217.
70. K. Urbas, M. Aleksandrzak, M. Jedrzejczak, R. Rakoczy, X. Chen & E. Mijowska, Nanoscale Research Letters, 2014, **9**, 656.
71. Z. Dahaghin, H. Z. Mousavi, and S. M. Sajjadi, Chem. Select , 2017, **2**, 1282-1289.
72. A. I. A. Sherlala, A. A. A. Raman and M. M. Bello, Environ. Technol., 2019, **40**, 1508-1516.
73. T. Szabó, L. Nánai, D. Nesztor, B. Barna, O. Malina and E. Tombácz, Advances in Mater. Sci. and Eng., 2018, **2018**, 11.
74. E. L. Albert, C. A. Abdullah, Y. Shiroshaki, Results in Phys. , 2018, **11**, 944-950.
75. V. Narayanaswamy , I. M. Obaidat , A. S. Kamzin , S. Latiyan, S. Jain , H. Kumar , C. Srivastava , S. Alaabed and B. Issa, Int. J. Mol. Sci., 2019, **20**, 3368.
76. P. Wu, Y. Wang, X. Hu, D. Yuan, Y. Liu and Z. Liu , J. Radioanalytical and Nuclear Chem., 2019, 319, 1111-1118.
77. G. Orfanakis, M. Patila, A. V. Catzikonstantinou, K.-M. Lyra, A. Kouloumpis, K. Spyrou, P. Katapodis, A. Paipetis, P. Rudolf, D. Gournis and H. Stamatis, Front Mater., 2018, **5**, 25.
78. X. Tang, P. Tang and L. Liu , J. Braz. Chem. Soc., 2018, **29**, 560-80.
79. D. R. Dreyer, S. Park, C. W. Bielawski and R. Ruoff, Chem. Soc. Rev., 2009, **39**, 228-240.
80. M. D. Dashtabi, H. Hekmatara and J. S. Yazdi, Mater. Chem. And Phy., 2019, **224**, 271-278.
81. H. Ge, C. Wang, S. Liu and Z. Huang, Bioresource Technology, 2016, **221**, 419-429.
82. M. Namvari and H. Namazi, Polymer Int., 2014, **63**, 1881-1888.
83. Maleki, Ali ,Hajizadeh, Zoleikha ,Abbasi and Hamid , Carbon Letters, 2018, **27**, 42-49.
84. S. Nigam ,K.C. Barick and D. Bahadur , J. Magn. Mater. , 2011, **323**, 237-243.
85. Q.-U. Ain, M. U. Farooq and M. I. Jalees, J. Water Process Eng., 2020, **33**, 101044.
86. Y. Zhang, H. L. Ma, Q. Zhang, J. Peng, J. Li, M. Zhai and Z. Z. Yu, J. Mater. Chem., 2012, **22**, 13064-13069.
87. S. Mu, G. Li, Y. Liang, T. Wu and D. Ma, Mater. Sci. Eng. C., 2017, **87**, 639-646.
88. Y. Xu, W. Hong, H. Bai, C. Li and G. Shi, Carbon, 2009, **47**, 3538-3543.
89. S. Stankovich, D. A. Dikin, R. D. Piner, K. A. Kohlhaas, A. Kleinhammes, Y. Jia, Y. Wu, S. T. Nguyen and R. S. Ruoff, Carbon, 2007,**45**, 1558-1565.
90. M. Adeli, A. Bahari and H. Hekmatara, Nano, 2008, **3**, 37.
91. V. Narayanaswamy , I. M. Obaidat , A. S. Kamzin , S. Latiyan , S. Jain , H. Kumar , C. Srivastava , S. Alaabed and B. Issa, Int. J. Mol. Sci., 2019, **20** , 3368.
92. X. Ji,Y. Xu, W. Zhang, L.Cui and J. Liu, Composites A: App. Sci. and Manufacturing, 2016, **87**, 29-45.
93. V. Ganesan , C. Louis and S. P. Damodaran, J. Environ. Chem. Eng., 2018, 6, 2176-2190.

94. J. Sun, Q. Liang, Q. Han, X. Zhang and M. Ding , Talanta, 2015, **132**, 557-563.
95. Y. Liu, H. Huang, D. Gan, L. Guo, M. Liu, J. Chen, F. Deng, N. Zhou, X. Zhang and Y. Wei, Ceremics Int., 2018, **44**, 18.
96. G. Sheng , Y. Li , X. Yang , X. Ren , S. Yang , J. Hu and X. Wang , RSC Adv., 2012, **2**, 12400-12407.
97. J. Liang, B. He, P. Li, J. Yu, X. Zhao, H. Wu, J. Li, Y. Sun and Q. Fan, Chem. Eng. J., 2018, **358**, 552-563.